Regime of Very High Confinement in the Boronized DIII-D Tokamak

G. L. Jackson, J. Winter, [a] T. S. Taylor, K. H. Burrell, J. C. DeBoo, C. M. Greenfield, R. J. Groebner, T. Hodapp, K. Holtrop, E. A. Lazarus, [b] L. L. Lao, S. I. Lippmann, T. H. Osborne, T. W. Petrie, J. Phillips, R. James, [c] D. P. Schissel, E. J. Strait, A. D. Turnbull, W. P. West, and DIII-D Team

General Atomics, San Diego, California 92128
(Received 23 August 1991)

Following boronization, tokamak discharges in DIII-D have been obtained with confinement times up to a factor of 3.5 above the ITER89-P L-mode scaling and 1.8 times greater than the DIII-D/JET H-mode scaling relation. Very high confinement phases are characterized by relatively high central density with $n_e(0) \approx 1 \times 10^{20}$ m^{-3}, and central ion temperatures up to 13.6 keV at moderate plasma currents (1.6 MA) and heating powers (12.5–15.3 MW). These discharges exhibit a low fraction of radiated power, $P \leq 25\%$, $Z_{\text{eff}}(0)$ close to unity, and lower impurity influxes than comparable DIII-D discharges before boronization.

PACS numbers: 52.55.Fa, 52.25.Fi, 52.25.Vy

In order to achieve ignition in proposed future fusion devices such as the Burning Plasma Experiment (BPX) and the International Thermonuclear Experimental Reactor (ITER), global energy confinement significantly better than the low-mode (L-mode) scaling relation is required in discharges with a low influx of impurities and low dilution of hydrogenic species [1]. Following boronization we have recently obtained discharges in the DIII-D tokamak with a very high confinement quiescent phase. These discharges have been repeated over many experimental days. We refer to this very high confinement phase as the VH mode. A number of tokamaks have obtained a high confinement mode (H mode) [2] with energy confinement times approximately a factor of 2 greater than for the L mode. In VH-mode discharges global energy confinement times are as much as a factor of 3.5 above ITER89-P [1] L-mode scaling and 1.8 times greater than the DIII-D/JET H-mode thermal confinement scaling relation [3]. This dramatic improvement in confinement quality is of great importance since the triple product $n_D T_i \tau_E$ (related to the ratio of fusion power to heating power) in a tokamak fusion system increases as the square of the confinement enhancement factor over the L-mode scaling. Moreover, the VH phase of these discharges has shown less radiated power loss than is usually observed in comparable quiescent, i.e., ELM-free, H-mode discharges. [Edge-localized modes (ELMs) are transient phenomena which can occur in the outer plasma region and produce enhanced particle and energy transport. H-mode behavior is often described by the presence or absence (quiescent phase) of ELMs.] Temperature and density profiles show steep edge gradients extending further into the plasma than in the normal H mode, indicating a thicker edge transport barrier region.

Boronization is a plasma-assisted chemical vapor deposition (CVD) process which deposits a thin, amorphous boron or boron-carbon film on all plasma facing components [4,5]. The boronization process was first implemented and later optimized in the TEXTOR tokamak at Forschungszentrum Jülich GmbH [4]. Boronization in DIII-D (in collaboration with Jülich) was accomplished using a glow discharge [6] in a helium-diborane gas mixture, 90% He and 10% B_2D_6, at a pressure of 5×10^{-3} mbar. A film of 100 nm average thickness was deposited. Depth profiles of a sample of the film taken by Auger electron spectroscopy (AES) and Ar-ion sputtering indicate that the film consists of about 90% B and 10% C. After boronization the spectral line intensities of impurity radiation were reduced tenfold to thirtyfold for metallic impurities and fivefold for carbon and oxygen during the beam-heated phase of the discharge when compared to previous operation. At the end of the Ohmic phase of a typical discharge after boronization, the ratios of the main impurity concentrations were B:C:O $\sim$ 2:1:1.

The thermal energy confinement time τ_{th} for VH-mode discharges, shown in Fig. 1, is 1.8 times larger than for standard ELM-free H-mode scaling in DIII-D. The abscissa in Fig. 1 is the empirical relation obtained from DIII-D/JET ELM-free scaling experiments using the major radius as the size scaling parameter [3]. Here τ_{th} is defined as $W_{\text{th}}/(P_T - \dot{W}_T)$, where W_{th} is the thermal plasma energy, excluding energy in nonthermal fast ions. P_T is the sum of the absorbed neutral beam power and Ohmic input power and $\dot{W}_T$ is the time rate of change of the total plasma energy. The thermal plasma energy was determined from the measured electron and ion temperatures (T_e, T_i), the electron density (n_e), and visible bremsstrahlung (Z_{eff}) profiles. The confinement time τ_{th} is calculated in the ELM-free phase of these discharges at the time where $\dot{W}_T/W_{\text{th}} \sim 0.3$ for the DIII-D and JET H-mode discharges and at $0.1 \leq \dot{W}_T/W_{\text{th}} \leq 0.5$ for VH-mode discharges. Because of the high density the energy content in fast ions in these plasmas is typically $\leq 15\%$.

VH-mode confinement has been obtained in deuterium double-null diverted discharges with deuterium neutral beam heating at 1.2 MA $\leq I_p \leq 1.6$ MA, and $B_T = 2.1$ T. These low-Z_{eff} discharges are characterized by a low fraction of radiated power, a significant bootstrap current in the plasma outer region, and a high edge pressure gra-
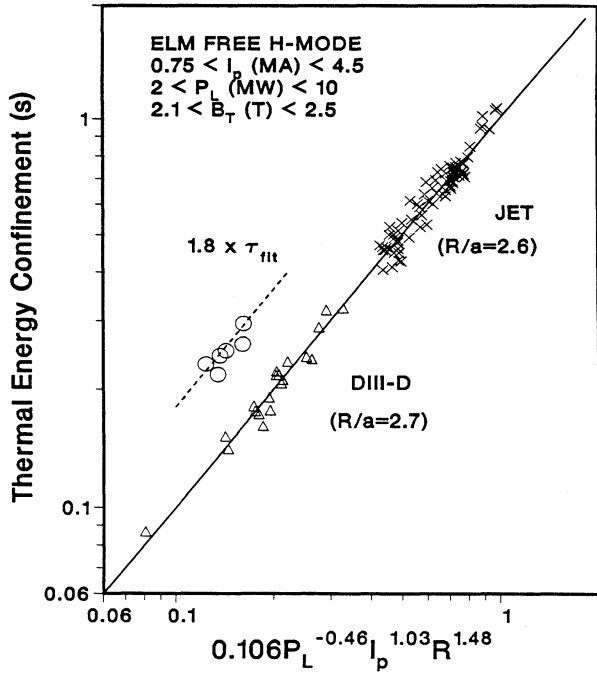
FIG. 1. VH-mode thermal energy confinement is an average of 1.8 times larger than that of ELM-free H modes in DIII-D and JET [3].

FIG. 2. Time-dependent development of a discharge with L-mode, VH-mode, and LM phases after the first boronization in DIII-D ($I_p = 1.6$ MA, $B_T = 2.1$ T, $\kappa = 2.08$, $q_{95} = 5.5$). An MHD instability occurs at ~ 3.62 sec, and the discharge then reverts to lower confinement with frequent ELMs. (a) The total plasma energy in MJ, (b) the neutral beam input and total radiation power in MW, (c) the line averaged density in m^{-3}, and (d) divertor D_α radiation.

dient. Ohmic target densities (just before beam heating) were low, $\bar{n}_e \leq 3 \times 10^{19}$ m^3. Discharges with higher target densities exhibited lower confinement, more typical of previous DIII-D H-mode discharges. A typical discharge is shown in Fig. 2. There is an L-mode phase during which the internal inductance slowly increases to $l_i \sim 1.3 \pm 0.16$ and strong sawtooth activity is observed. Within the error bars, this l_i is no higher than for similar tokamak discharges before boronization with a long L-mode period. Although the discharge shown in Fig. 2 had a long L-mode phase of 1.25 sec, other VH-mode discharges have had L-mode phases as short as 40 msec. Once a VH-mode transition occurs in these 1.6-MA discharges, there is little or no sawtoothing activity and quiescent periods of up to 700 msec have been observed.

The VH-mode transition requires higher beam power than for the H mode. In Fig. 2 the transition occurs after the neutral beam heating power is increased to 12.5 MW. Although increased auxiliary power facilitates the L to VH transition, VH-mode discharges have also been achieved with a constant neutral beam power of 9.4 MW at 1.6 MA. No VH mode has been obtained yet in a single-null configuration with the grad$B$ drift toward the X point; all of the discharges reported here are in a double-null configuration. Previous investigations in DIII-D have shown that the power level required for an L- to H-mode transition is ~ 2 times higher for an upper single-null divertor than for an H-mode transition in the lower single-null configuration where the grad$B$ drift is

towards the X point and $P_{L \to H} \sim 2$ MW at 1.6 MA and 2.1 T [7,8]. The L to VH transition power threshold is greater than either lower single-null or double-null L to H power thresholds. The VH-mode phase is terminated by the appearance of frequent ELMs, and the stored energy, electron temperature, and density relax to lower levels while radiated power on axis increases.

Immediately after the L to VH transition, the fraction of total radiated power, $P_{\text{rad}}/P_{\text{aux}}$, inferred from a 21-channel bolometer array, is 5% to 25% and a peaking of radiated power on axis is not observed during the VH-mode phase. This fraction is lower than the standard quiescent H-mode discharges, and does not increase appreciably unless MHD activity commences. This reduction of radiated power is not sufficient, taken alone, to explain the improvement in energy confinement.
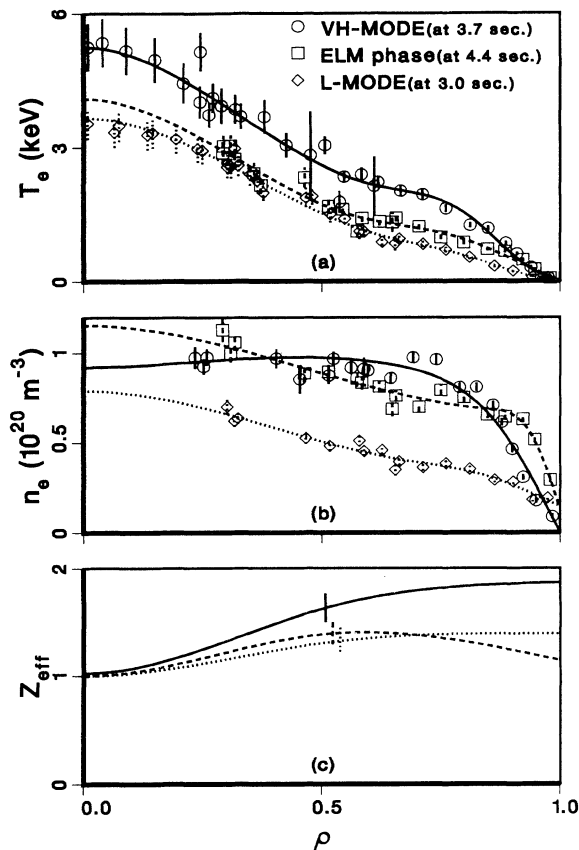
FIG. 3. (a) A high electron temperature (T_e) gradient extending into $\rho < 0.8$ is observed during VH mode (———) when compared to L (·····) and ELM (---) phases of the same discharge ($I_p =1.6$ MA, $B_T =2.1$ T, $\kappa =2.06$). T_e is determined from Thomson scattering and third-harmonic electron-cyclotron emission. In (b) and (c) electron density (n_e) and Z_{eff} profiles are shown.

Electron temperature and density profiles from the multipulse Thomson scattering system are shown in Fig. 3 for the L-mode, VH-mode, and post-VH ELM phases of a discharge after boronization. During the VH mode there are both high temperature and density gradients extending inward to $0.8 \leq \rho < 1.0$. The normal H mode exhibits large edge T_e and n_e gradients, indicating an edge region of reduced transport [9], but not as extensive as for the VH mode. When the transition into the VH mode occurs after a short L-mode phase at low density, values of central ion temperature T_i as high as 13.6 keV and central electron temperature $T_e =5.6$ keV were observed.

The axisymmetric MHD equilibrium is reconstructed consistent with the kinetic, external magnetic, and motional Stark effect data. The results of the equilibrium reconstruction for the VH-mode discharge in Fig. 2 near the beta limit are shown in Fig. 4. As seen from the cross section of the poloidal flux contours, this is a high triangularity $(\delta =0.83)$, elongated $(\kappa =2.1)$, double-null
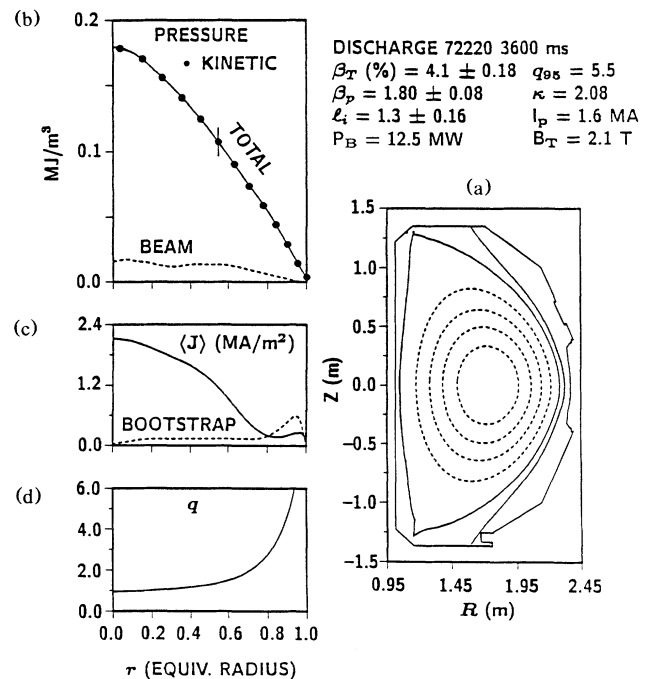
FIG. 4. (a) MHD analysis of the VH-mode MHD equilibrium reconstructed from magnetic, motional Stark effect, and kinetic data; (b) plasma pressure profile with calculated beam ion profile; (c) current density profile with bootstrap current density profile; and (d) q, or safety factor, profile.

divertor. The safety factor at 95% of enclosed poloidal flux is $q_{95} =5.5$. The pressure profile shown in Fig. 4 is obtained from measurements of the electron temperature, ion temperature, electron density, visible bremsstrahlung, and a calculation of the fast ion pressure. The solid points in Fig. 4 represent the calculated pressure from spline fits to experimental measurements with the calculated fast ion pressure added. The line is the pressure profile obtained from the full equilibrium analysis. The plasma energy calculated from integrating the measured kinetic profiles plus the fast ions is 2.5 MJ which agrees with the energy from the MHD analysis, $W_{\text{MHD}} =2.5$ MJ, and that determined from diamagnetic loop measurements, $W_{\text{dia}} =2.45$ MJ. Of particular note is the relatively high current density near the boundary, which is consistent with the calculated bootstrap current driven by the large edge pressure gradient. The bootstrap current is calculated to be a third of the total current.

The termination of the ELM-free VH phase in the discharge shown in Fig. 4 is due to a stability limit and not confinement or transport limitations. Before the first ELM, magnetic fluctuations increase, and MHD activity, soft-x-ray profiles, and stability analysis indicate that the discharge behavior is consistent with the onset of an internal kink. The flux-surface-averaged current density is shown in Fig. 4 for a discharge with the highest ob-

served β_T at $I_p = 1.6$ MA. Immediately after the time shown in Fig. 4, magnetic fluctuations increase and β_N $= \beta_T a B_T/I_p$ reaches 3.6% mT/MA. This limit to the increase in pressure by pressure-driven kinks is expected in plasmas with high internal inductance and large edge bootstrap currents [10,11]. Following this MHD event, energy confinement decreases, approaching a more conventional H-mode discharge with frequent ELMs. Other discharges at lower power avoid this MHD instability, although a relaxation to a lower confinement ELM phase is observed. With moderate plasma current (1.6 MA) the following parameters have been achieved in VH-mode discharges:

Discharge	P_{NBI} (MW)	$n_D(0)$ $(10^{20}$ m$^{-3})$	$T_i(0)$ (keV)	$T_e(0)$ (keV)	τ_{th} (sec)
72220 (boronization No. 1)	12.5	0.89	6.35	5.5	0.24
72523 (boronization No. 2)	15.3	0.79	13.6	5.6	0.25

After the second boronization, a hot-ion H mode was achieved with the highest $n_D(0)T_i(0)\tau_{th}$ observed to date in DIII-D, 2.7×10^{20} m^{-3}keV sec.

Further work is needed to clarify the cause of confinement improvement in the VH mode. Necessary conditions for the VH mode appear to be $Z_{eff} \sim 1$, low target density, low neutral pressure, and $P_{rad}/P_{aux} \leq 0.25$. While boronization produced these conditions, its role in the confinement improvement is unclear. We are investigating the apparently thicker edge transport barrier, the role of the unusually peaked current profile, the large edge bootstrap current, and the tendency of the VH mode to have a larger edge temperature increase than seen in the H mode.

We speculate that an electric-field shear region [12,13] of greater thickness might be the source of the improved confinement; our data at present are consistent with this idea. However, we cannot make a definitive statement, since the electric-field shear region in VH-mode plasmas is broader than we can measure with our present system. We are in the process of improving our measuring capability and the results will be reported in a future publication.

The utility of the VH-mode confinement regime awaits future work extending it to higher plasma current, steady-state operation, and developing a more detailed understanding of the physics involved. If steady-state VH-mode discharges, perhaps with some ELM activity, can be obtained, the utilization of this high confinement regime would increase the performance of future large fusion devices, relax engineering constraints, and provide an additional margin to accomplish ignition.

(a)Permanent address: Forschungszentrum Jülich, Association EURATOM-Kernforschungsanlage Jülich, Jülich, Germany.
(b)Permanent address: Oak Ridge National Laboratory, Oak Ridge, TN 37830.
(c)Permanent address: Lawrence Livermore National Laboratory, Livermore, CA 94550.

[1] P. N. Yushmanov et al., Nucl. Fusion 30, 1999 (1990).
[2] R. D. Stambaugh et al., Phys. Fluids B 2, 2941 (1990).
[3] D. P. Schissel et al., Nucl. Fusion 31, 73 (1991).
[4] J. Winter et al., J. Nucl. Mater. 162-164, 713 (1989).
[5] J. Winter, J. Nucl. Mater. 176-177, 14 (1990).
[6] G. L. Jackson et al., Nucl. Fusion 30, 2305 (1990).
[7] F. Hinton, Nucl. Fusion 25, 1457 (1985).
[8] K. H. Burrell et al., Plasma Phys. Controlled Fusion 31, 1649 (1989).
[9] F. Wagner et al., Phys. Rev. Lett. 53, 1453 (1984).
[10] T. S. Taylor et al., in Plasma Physics and Controlled Nuclear Fusion Research, 1990 (International Atomic Energy Agency, Vienna, 1991), Vol. 1, p. 177.
[11] L. Lao et al., in Proceedings of the Eighteenth European Conference on Controlled Fusion and Plasma Physics, Berlin, Germany, 1990 (European Physical Society, Petit-Lancy, Switzerland, 1991), Vol. 15C, Pt. IV, p. 73.
[12] R. J. Groebner et al., in Plasma Physics and Controlled Nuclear Fusion Research, 1990 (Ref. [10]), Vol. 1, p. 453.
[13] E. J. Doyle et al., Phys. Fluids B 3, 2300 (1991).